Characterization of the photoneutron flux emitted by an electron accelerator using an activation detector

Adrien Sari, Mathieu Agelou, Igor Bessières, Frédérick Carrel, Mehdi Gmar, Frederic Lainé, A. Lyoussi, Stéphane Normand, Aimé Ostrowsky, Line Sommier

Characterization of the Photoneutron Flux Emitted by an Electron Accelerator Using an Activation Detector

Adrien Sari, Mathieu Agelou, Igor Bessières, Frédérick Carrel, Mehdi Gmar, Frédéric Lainé, Abdallah Lyoussi, Stéphane Normand, Aimé Ostrowsky, and Line Sommier

***Abstract*—Electron accelerators are intense photoneutron sources for nuclear waste packages characterization and homeland security applications. Moreover, when considering medical accelerators, photoneutrons can cause secondary cancers for patients and also expose hospital staff to deactivation gammas after the irradiation. In this study, we investigate photoneutrons properties according to average emission intensity, energy spectrum and spatial distribution. The latter parameter was measured using an activation detector and the other two parameters were determined by simulation, and then, evaluated by comparing absolute activation simulations and measurements. Our methodology was applied to characterize the photoneutron flux generated by two electron accelerators. Our study has shown that there is a strong probability for photonuclear cross-sections to be undervalued in the energy range studied.**

I. Introduction

WHEN electrons irradiate heavy nuclei, high-energy photons are created by Bremsstrahlung. In turn, photons can react with the nuclei and produce neutrons called photoneutrons. An accurate knowledge of the photoneutron flux produced by an electron accelerator is of major interest for different applications such as radiation therapy [1], [2], homeland security [3], [4], and nuclear waste packages characterization [5], [6]. Although these applications require different types of accelerators, the photoneutron fluxes generated are similar. Our aim was to determine a single photoneutron beam characterization methodology which could be applied in these application fields. In our approach, the photoneutron flux was characterized according to three parameters: average emission intensity, energy spectrum and spatial distribution. The latter parameter was measured using an activation detector [7] designed by simulation with MCNPX [8], [9], and optimized for measuring such photoneutron beams. First, the activation detector containing a foil of material is irradiated by photoneutrons, and then, deactivation photons emitted by the foil are detected with a germanium detector. Average emission intensities and energy spectra were determined by simulation. Finally, these two parameters were evaluated by comparison between absolute activation simulations and measurements.

Our characterization method has been applied on two accelerators, both owned by CEA LIST: the accelerator of the SAPHIR facility which is used for research on nuclear waste packages characterization techniques; and a metrological Saturne 43F medical accelerator designed by General Electric which is used for calibration of French hospitals' ionization chambers and research in radiation therapy. For each accelerator, measurements were carried out for two electron energies and foils of different materials were tested. First, we present the simulation study intended to design a photoneutron activation detector. Then, we present the study dedicated to the characterization of the photoneutron flux emitted by the electron accelerator of the SAPHIR facility. Finally, we present the photoneutron flux characterization study carried out for the Saturne 43F medical accelerator.

Manuscript received June 14, 2012. A. Sari, M. Agelou, I. Bessières, F. Carrel, M. Gmar, F. Lainé, S. Normand, A. Ostrowsky and L. Sommier are with CEA, LIST, F-91191, Gif-sur-Yvette, France (e-mail: adrien.sari@cea.fr). A. Lyoussi is with CEA, DEN, F-13108 Saint-Paul-Lez-Durance, France.

II. Design of an Activation Detector

Fast neutron fluxes emitted by electron accelerators can be measured using large neutron capture cross-section material leading to a radioactive daughter nucleus with suitable life-time [7]. First, neutrons are thermalized (in polyethylene for instance), and then, activate a foil of material. An activation detector scheme is presented in Fig. 1. We considered foils made of vanadium, silver or aluminum. For each material, Table I gathers: the stable isotope of interest, its abundance, the radioactive isotope created, (n,γ) thermal cross-section, radioactive isotope half-life time, and energy of the deactivation gamma-ray of interest. It is important to notice that the weak 633 keV gamma-ray emission probability following deactivation of ^{108}Ag is offset by a high (n,γ) cross-section on ^{107}Ag. We simulated the (n,γ) reaction rate in the foil for different thicknesses of polyethylene between the front side of the detector (side facing the neutron source) and the foil (same polyethylene thickness in front of and behind the foil). The fast neutron source used in these simulations was similar to the one determined in a previous study [6]. Fig. 2 presents our results obtained for a foil of vanadium (statistical uncertainties lower than 1%) and shows that 6 cm of polyethylene is appropriate, as illustrated in Fig. 1. Simulations conducted for a foil of silver or aluminum lead to the same conclusion. We evaluated by simulation the interest of surrounding the detector with a 1 mm thick cadmium cover. We showed that impact of the cadmium cover on the thermal part of the fast neutron source is negligible and that neutrons scattered by the walls of the irradiation hall, which have sufficient energy to penetrate cadmium, do not affect significantly the (n,γ) reaction rate in the foil. Overall, the cadmium cover enables to restrict activation of the foil to neutrons thermalized inside the detector and enables to run

simulations faster as simulation of irradiation hall is then not necessary.

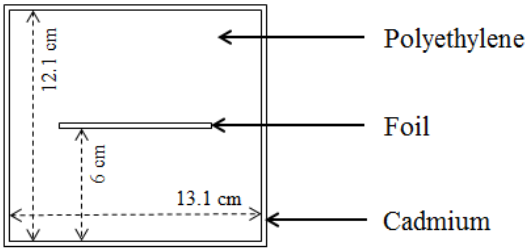

Fig. 1. Scheme of an activation detector.

TABLE I
MAIN CHARACTERISTICS OF THE RADIOACTIVE ISOTOPE OF INTEREST PRODUCED FURTHER TO NEUTRON ACTIVATION OF THE VANADIUM, SILVER, OR ALUMINUM FOIL [10], [11].

	Vanadium	Silver	Aluminum
Stable isotope	^{51}V	^{107}Ag	^{27}Al
Abundance (%)	99.75	51.84	100.00
Radioactive isotope	^{52}V	^{108}Ag	^{28}Al
(n,γ) thermal cross-section (b)	4.92	37.60	0.23
Half-life time (min)	3.74	2.37	2.24
Gamma energy (keV)	1434.06	632.98	1778.85
Emission probability	100.00%	1.76%	99.98%

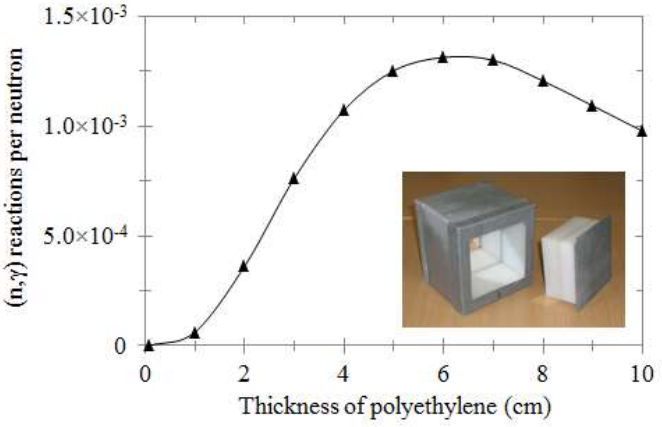

Fig. 2. Optimization of the thickness of polyethylene between the front side of the detector and the foil, and activation detector containing a foil of silver in its open position (front side of the activation detector removed).

The activation detector built further to our simulation study, shown in Fig. 2, is 12.1 cm long (6 cm of polyethylene in front of and behind the foil), 13.1 cm large and 14.1 cm high. The cadmium cover is 0.7 mm thick. Foils are 10 × 10 cm² and 1 mm thick. As certified by the supplier (Goodfellow), their purity is 99.9% or higher depending on the material. The front side of the detector is removable in order to place or remove easily the foil in the detector, as can be seen in Fig. 2.

III. CHARACTERIZATION OF THE PHOTONEUTRON FLUX EMITTED BY THE ACCELERATOR OF THE SAPHIR FACILITY

The SAPHIR facility, owned by CEA LIST, is located in Saclay (France). SAPHIR houses a linear electron accelerator used for research and development projects which deal with nuclear waste packages characterization [12]. Experiments were conducted for two mean energies of electron spectrum: 14 MeV and 17 MeV. Peak current was 100 mA with 2.5 µs pulse duration and 50 Hz repetition frequency. As tungsten photonuclear cross-sections threshold errors have been brought to light in a previous study [6], we carried out measurements for two targets of 1 cm thickness and 5 cm diameter: one made of tungsten (99.95% purity) and one made of tantalum (99.9% purity).

A. Angular distribution

We measured the angular distribution of the photoneutron flux with our activation detector. First, the latter was placed in front of the target at 75 cm of distance, and then, moved onto different positions located along the arc of a 75 cm radius circle. Fig. 3 illustrates the principle of the measurement. For each position, the activation detector was irradiated during 10 min. After 2 min of cooling time, deactivation gamma spectra were acquired during 10 min. During the acquisition, the activation detector was placed in its open position in front of a germanium detector in such a way that the irradiated side of the activation detector was in front of the germanium detector. The front side of the activation detector and the germanium detector were separated by 9 cm (15 cm between the foil and the germanium detector). We used a p-type HPGe detector (ORTEC, GEM40P-PLUS) which presents a 40% relative efficiency, linked to a DSPECPro digital gamma-ray spectrometer (ORTEC).

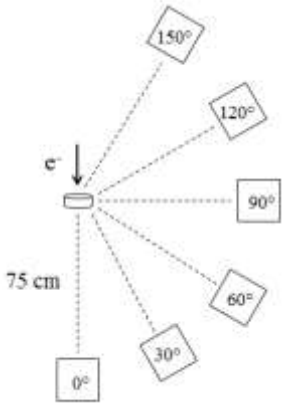

Fig. 3. Representation of the angular distribution measurement at the SAPHIR facility.

We showed by simulation that, when the activation detector is exposed to high-energy photons (in positions 0°, 15°, and to a lesser extent, in position 30°), spurious neutrons are produced by photonuclear reactions in the foil and in the cadmium surrounding the detector, though contribution from cadmium is the highest. We have verified that production of spurious neutrons by photonuclear reactions in the polyethylene of the detector and in the air of the irradiation hall can be neglected. Furthermore, when conducting measurements with a foil of silver, a second mechanism of the production of the radioactive isotope of interest interferes (production of ^{108}Ag by (γ,n) reaction on ^{109}Ag). These effects lead to a forward peaking in the angular distribution measured. As an example, we present in Fig. 4 the angular distribution of the photoneutron flux produced by a tantalum target irradiated by 17 MeV electrons, measured with a foil of vanadium, silver, or aluminum. All angular distributions presented are normalized at one in position 60° and error bars are omitted for clarity (statistical uncertainties at one sigma on net peak areas are between 0.2% and 4.5%). When subtracting by simulation the spurious effects discussed previously, the forward peaking of the angular distributions disappears.

Neutrons, known as electroneutrons, can be produced by electronuclear reactions in the target. However, few experimental data exist on (e,n) reactions. Data were published by M. I. C. Cataldi *et al.* [13] for ^{181}Ta in 1988. As no data have ever been published on the electroneutron angular distribution, K. Kosako *et al.* [14] assumed that the angular distribution was similar to the one of Bremsstrahlung photons, which means that electroneutrons should mainly be emitted in the forward direction. Nevertheless, electronuclear reaction cross-sections are low in comparison with photonuclear reaction cross-sections and simulations showed that the forward peaking of the angular distribution measured with the activation detector can be attributed to production of photoneutrons in the cadmium of the detector and the foil.

Fig. 5 shows the angular distribution measured with a foil of vanadium for two electron energies: 14 MeV and 17 MeV. Shape of the angular distribution obtained at both energies is similar. However, as expected, the forward peaking of the angular distribution is stronger for 17 MeV electrons. Indeed, the higher the energy, the more spurious photoneutrons is produced in the cadmium and the foil. We can also notice that the target-stand has little effect on the angular distribution. We also compared the angular distribution obtained for a tantalum and a tungsten target. Due to the fact that tungsten has a higher density than tantalum, less high-energy photons escape from the tungsten target than the tantalum one, which means that fewer neutrons are produced in the cadmium and the foil when considering a target made of tungsten. Finally, we have shown that neutrons produced by the conversion target are overall emitted in an isotropic manner.

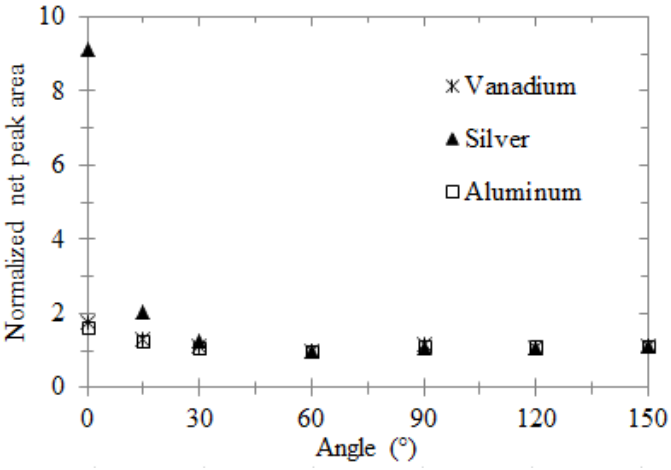

Fig. 4. Angular distribution of the photoneutron flux emitted by a tantalum target irradiated by 17 MeV electrons, activation detector containing a foil of vanadium, silver, or aluminum.

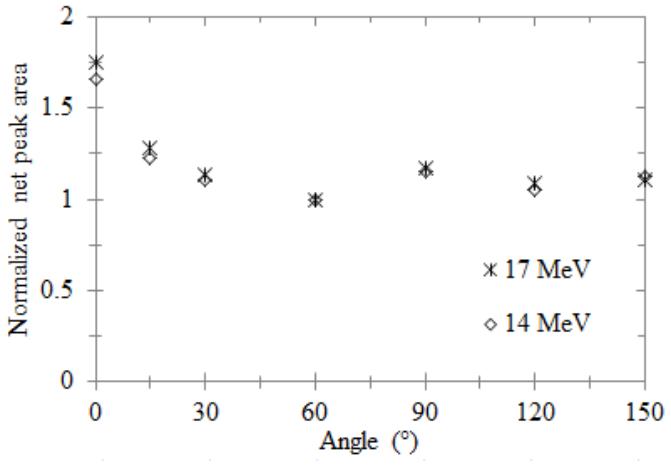

Fig. 5. Angular distribution of the photoneutron flux emitted by a tantalum target irradiated by 14 MeV or 17 MeV electrons, activation detector containing a foil of vanadium.

B. Energy spectrum and average emission intensity

We simulated the photoneutron energy spectrum for the tungsten or tantalum target irradiated by 14 MeV or 17 MeV electrons. By way of illustration, energy spectra obtained for the tungsten target are shown in Fig. 6. Results obtained for the tantalum target are similar. The mean energy is around 1 MeV for both electron energies. As photoneutrons are mainly emitted by an evaporation process, the shape of the spectra is a typical Maxwell-Boltzmann curve presenting a maximum at 0.5 MeV which corresponds to the nuclear temperature [15].

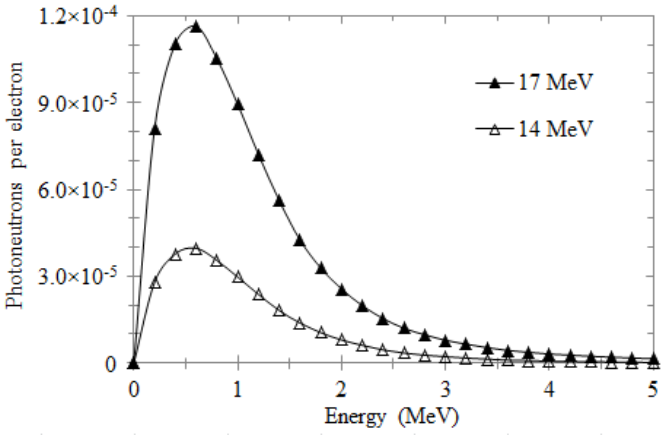

Fig. 6. Energy spectra of the photoneutron flux emitted by a tungsten target irradiated by 14 MeV or 17 MeV electrons.

For the tungsten target, average emission intensities were calculated from (γ,n) + 2(γ,2n) composed reaction rates using CNDC cross-sections [16], as recommended in a previous paper in order to avoid cross-sections threshold errors [6]. For the tantalum target, average emission intensities were calculated from (γ,xn) reaction rates using ENDF/B-VII cross-sections [17] after having verified that no (γ,xn) cross-section threshold error appears in this database for ^{181}Ta. Statistical uncertainties associated to our reaction rates simulations are lower than 0.01%. Simulations dedicated to the reaction rates calculations were conducted considering the electron spectrum measured at the SAPHIR facility. Average emission intensities were obtained by multiplying the (γ,xn) reaction rates (number of neutrons produced per electron) by the number of electrons delivered by the accelerator per second (6.25×10^{17} e^-/s), by the pulse duration (2.5 µs), and by the frequency (50 Hz). Results obtained are presented in Table II.

TABLE II
AVERAGE EMISSION INTENSITY OF THE PHOTONEUTRON FLUX EMITTED BY A TUNGSTEN OR TANTALUM CONVERSION TARGET IRRADIATED BY 14 MEV OR 17 MEV ELECTRONS.

	14 MeV	17 MeV
Tungsten	2.72×10^{10} n/s	7.69×10^{10} n/s
Tantalum	2.33×10^{10} n/s	6.53×10^{10} n/s

In order to evaluate the accuracy of energy spectra and average emission intensities, both determined by simulation, we compared absolute activation calculations with our measurements. Net peak areas were calculated with the following equation:

$$S_\gamma = \tau_{(n,\gamma)}\, \varepsilon_\gamma\, p_\gamma\, \frac{1-e^{-n\lambda T}}{1-e^{-\lambda T}}\, t_1\, e^{-\lambda t_2}\left(1-e^{-\lambda t_3}\right)$$

In the latter, S_γ is the net peak area (in counts), $\tau_{(n,\gamma)}$ is the (n,γ) reaction rate (number of (n,γ) reactions per second), ε_γ is the absolute detection efficiency of HPGe detector, p_γ is the emission probability of the gamma-ray of interest, n is the number of pulses during the irradiation (30000 pulses), λ is the decay constant (s^{-1}), T is the pulse period (20 ms), t_1 is the pulse duration (2.5 µs), t_2 is the cooling time (2 min), and t_3 is the counting time (10 min). As reaction rates are normalized by incident electron in MCNPX, $\tau_{(n,\gamma)}$ is obtained by multiplying the reaction rate simulated by the number of electrons generated by the accelerator per second (6.25×10^{17} electrons per second). The absolute detection efficiency of the gamma-ray of interest was simulated using a model of our germanium detector.

First, in order to determine the overall uncertainty on the pulse duration, the frequency and the electron current peak intensity, we compared simulation and experiment based on photofission of uranium samples. Measurements were carried out by counting delayed neutrons using ^{3}He detectors surrounded by polyethylene and cadmium. Different samples were irradiated. For both electron energies considered in this study, simulations overestimated experimental results by 14%. Then, the MCNPX model of our germanium detector was evaluated by comparison of simulations and measurements using ^{60}Co, ^{137}Cs and ^{152}Eu punctual sources. In the gamma-ray energy of interest, simulated absolute detection efficiencies overestimates the ones obtained experimentally by 8%. Statistical uncertainties associated to reaction rates and absolute detection efficiencies are respectively between 1% and 3%, and lower than 0.4%. For the tantalum and the tungsten targets, calculated net peak areas include the two correction factors discussed previously. For calculations involving the tungsten target, a third correction factor is also taken into account as the photoneutron yield is underestimated in our simulations as we used ENDF/B-VII photonuclear cross-sections [6]. As brought to light in a previous study [6], this correction factor on tungsten photonuclear cross-section threshold errors can be determined by calculating the gap between a (γ,n) + 2(γ,2n) composed reaction rate using CNDC cross-sections and a (γ,xn) reaction rate using ENDF/B-VII cross-sections in a target made of tungsten. The gap was obtained considering the electron energy spectrum of the accelerator. To take into account third correction factor in our calculations carried out with the tungsten target, net peak areas obtained by simulation are multiplied by 1.278 at 14 MeV and 1.171 at 17 MeV. Ratios between calculated and experimental net peak areas are determined for each angular position. However, only three positions are retained to calculate mean values — positions 60°, 120° and 150° — in which the activation detector is outside the high-energy photon beam and target-stand effects are weak. We compared simulations carried out for two different (n,γ) cross-section libraries: ENDF/B-VI [18] and ENDL-92 from Lawrence Livermore National Laboratory. The mean values are presented in Table III for 14 MeV or 17 MeV electrons.

TABLE III
RATIOS BETWEEN SIMULATED AND EXPERIMENTAL NET PEAK AREAS CARRIED OUT FOR THE ACTIVATION DETECTOR CONTAINING A FOIL OF VANADIUM, SILVER, OR ALUMINUM. THE TUNGSTEN OR THE TANTALUM TARGET WERE IRRADIATED BY 14 MEV OR 17 MEV ELECTRONS AND SIMULATIONS WERE CARRIED OUT USING ENDL-92 OR ENDF/B-VI (n,γ) CROSS-SECTIONS.

		ENDL-92			ENDF/B-VI		
		V	Ag	Al	V	Ag	Al
14 MeV	Tungsten	0.65	0.88	0.56	0.56	0.98	0.65
	Tantalum	0.66	0.96	0.51	0.56	1.09	0.59
17 MeV	Tungsten	0.57	0.86	0.44	0.52	0.92	0.49
	Tantalum	0.56	0.85	0.43	0.51	0.90	0.47

From results presented in Table III, several comments can be made. Generally speaking, simulation underestimates experiment nearly by a factor of two which is in good agreement with K. Kosako *et al.* [14] who found 50%-150% underestimation for absolute activation calculations carried out for 18 MeV electrons. However, they considered different activation reactions than the ones studied in this article. We can also notice that simulations carried out for a foil of silver seem to be in better agreement with experiment than the ones conducted for vanadium or aluminum. In fact, it is likely that (n,γ) cross-sections on ^{107}Ag from both ENDL-92 and ENDF/B-VI are overvalued. Furthermore, disagreements between simulation and measurement are stronger for 17 MeV electrons than for 14 MeV electrons and gaps between ratios using either ENDL-92 or ENDF/B-VI (n,γ) cross-section libraries are within 13%. When considering same foil and same energy, discrepancies between simulation and experiment carried out for the tungsten or the tantalum target are similar which tends to show that accuracy of photonuclear cross-section evaluation is similar for these two materials (correction factor on tungsten photonuclear cross-section threshold errors taken into account). Finally, discrepancies between simulation and measurement remain. There is a strong probability for the latter to be due to tungsten and tantalum photonuclear cross-sections undervaluation in the energy range of interest, which means that simulations underestimate photoneutron production.

IV. CHARACTERIZATION OF THE PHOTONEUTRON FLUX EMITTED BY A SATURNE 43F MEDICAL ACCELERATOR

Performance of our photoneutron flux characterization method has been evaluated on a Saturne 43F medical accelerator designed by General Electric. Experiments were carried out at Laboratoire National Henri Becquerel (CEA LIST) which is located in Saclay (France). This metrological electron accelerator is mainly used for research in radiation therapy and calibration of French hospitals' ionization chambers, thus guaranteeing high stability photon beam. Measurements were conducted for 12 MV and 20 MV photons (electron accelerating voltage of 12 MV and 20 MV which means that maximum energy of Bremsstrahlung-photon spectrum is respectively of 12 MeV and 20 MeV) irradiating a 10 × 10 cm² field (at 1 m from the conversion target). When delivering 12 MV and 20 MV photons, peak current was 10 mA and 30 mA with 4 µs pulse duration and 100 Hz repetition frequency.

A. *Profile*

We chose to determine the spatial distribution of the photoneutron flux emitted by the Saturne 43F medical accelerator according to a radiation therapy profile. The activation detector was positioned at one meter in front of the target in the photon field and moved onto different positions situated perpendicularly to the electron beam axis. Apart from that, experimental protocol is similar to the one used at the SAPHIR facility. Fig. 7 presents photoneutron profiles for 20 MV photons measured with the activation detector containing a foil of silver or vanadium. Profiles are normalized at one in position 10 cm (position in which the activation detector is not irradiated by high-energy photons). Statistical uncertainties are negligible. When ignoring position 0 cm, both materials give the same profile. We verified that, when considering 12 MV photons, although less high-energy photons interfere for the measurement conducted with a foil of silver in position 0 cm than the one at 20 MV, the shape of the photoneutron profile is similar. Profiles obtained with a foil of vanadium for 12 MV and 20 MV photons are compared in Fig. 8 (statistical uncertainties negligible). The profiles are normalized at one for position 0 cm. Both profiles give the same tendency. They diminish gradually from the photon field to the periphery in such a way that twice fewer neutrons are detected at one meter from the photon field.

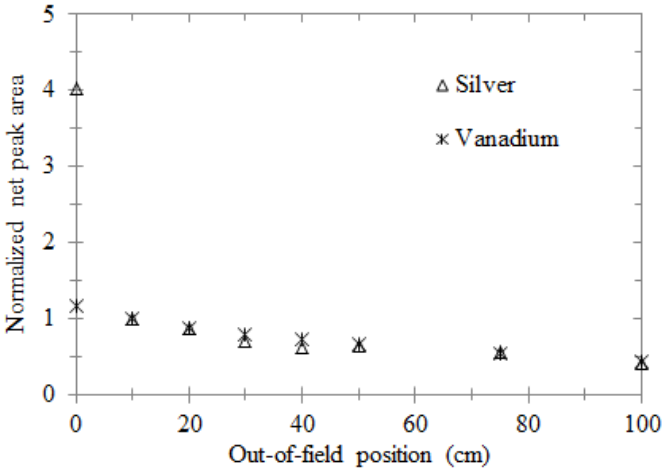

Fig. 7. Photoneutron profiles measured at the Saturne 43F medical accelerator for 20 MV photons, activation detector containing a foil of silver or vanadium.

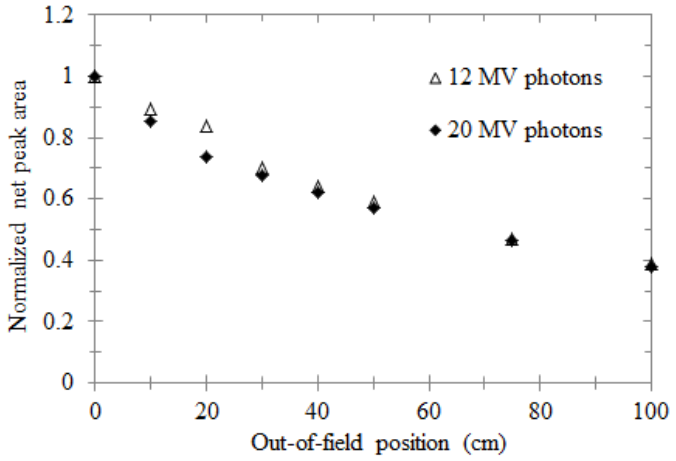

Fig. 8. Photoneutron profiles measured at the Saturne 43F medical accelerator with an activation detector containing a foil of vanadium for 12 MV or 20 MV photons.

B. MCNPX model evaluation

The Saturne 43F medical accelerator has a complex geometry in comparison with the one of the electron accelerator of the SAPHIR facility. Graphic representations of the MCNPX models for 12 MV and 20 MV photons are shown in Fig. 9. Main components are indicated. Apart from electron energy spectrum, the only difference between these two models is the flattening filter. First, we determined materials on which photonuclear reactions leading to the emission of photoneutrons occur and localization of these reactions in the accelerator. These estimations were carried out according to a one meter square plane placed in front of the accelerator at one meter from the target. We showed that photonuclear reactions on isotopes of tungsten and lead account for most of the photoneutron yield in the two models. As can be seen in Table IV, photoneutrons are mainly produced in the jaws, the primary collimator, and the target.

Secondly, we evaluated our MCNPX model of the Saturne 43F accelerator by comparison of simulations and measurements. We simulated the profile measurement and compared the latter with the experimental results. Disagreements between simulation and experiment appeared in the axis and in the most peripheral positions. In order to explain these discrepancies, for each position of the activation detector, we identified localization of production of photoneutrons in the accelerator and materials involved. For illustration, few results obtained for the 20 MV photon model are shown in Fig. 10. We clarified that the increase of the contribution of the target in position 75 cm and 100 cm is not physically correct as external elements that are not simulated mask the target. Results obtained after having subtracted the target contribution in these two positions are presented in Fig. 11 and Fig. 12 for 12 MV and 20 MV photons respectively. Better agreement is obtained in these remote positions.

Regarding disagreement in position 0 cm, different assumptions were tested. This disagreement could be due to the fact that contribution from materials to the production of photoneutrons is different between field and out-of-field positions (when considering the corrected models). Contribution of tungsten is higher in the photon field than in the peripheral positions and conversely for lead. It is also possible that contributions from the cadmium surrounding the detector and the foil to the production of photoneutrons are too high in comparison with potential underestimated photoneutron production by the accelerator due to poor (γ,xn) cross-section knowledge in the energy range studied.

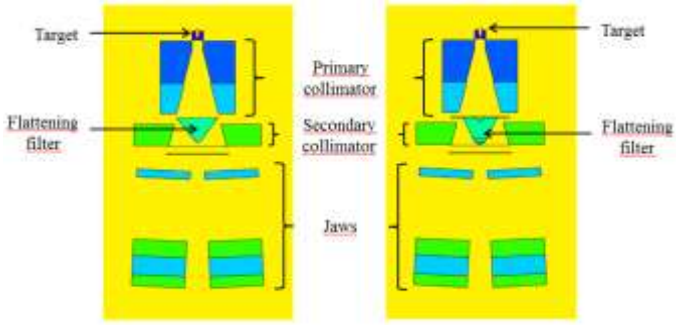

Fig. 9. Graphic representations of the MCNPX models. On the left: 12 MV photon model. On the right: 20 MV photon model.

TABLE IV
CONTRIBUTION OF COMPONENTS TO THE PRODUCTION OF PHOTONEUTRONS BY THE SATURNE 43F ACCELERATOR FOR 12 MV OR 20 MV PHOTONS.

	12 MV photons	20 MV photons
Target	15.4%	15.4%
Primary Collimator	15.4%	20.2%
Secondary Collimator	3.5%	3.1%
Flattening filter	0.5%	3.3%
Jaws	64.4%	55.6%
Other	0.8%	2.4%

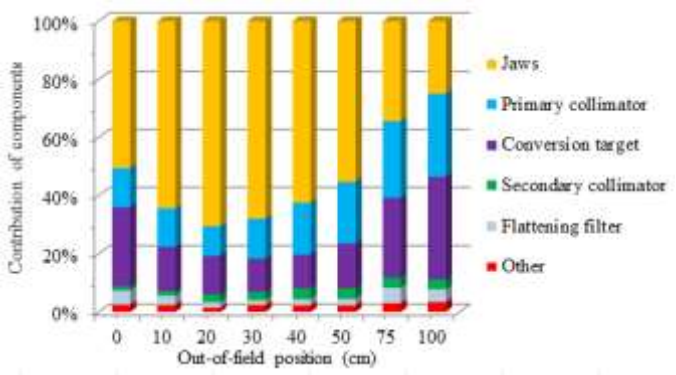

Fig. 10. Contribution of the accelerator components in each position of the photoneutron profile for 20 MV photons.

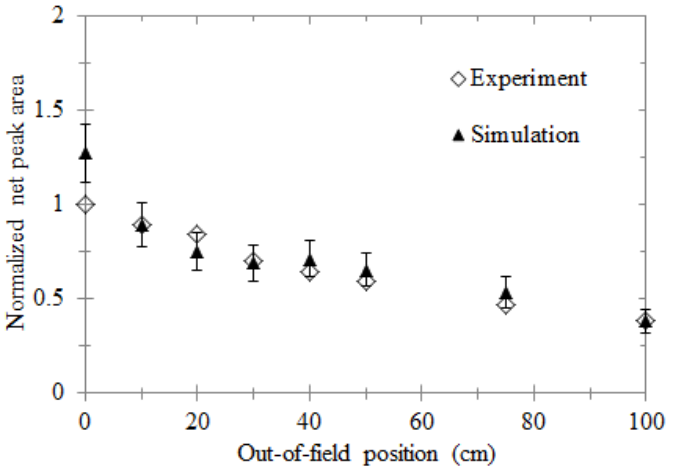

Fig. 11. Comparison between simulated and measured photoneutron profiles for 12 MV photons, simulation model corrected, activation detector containing a foil of vanadium.

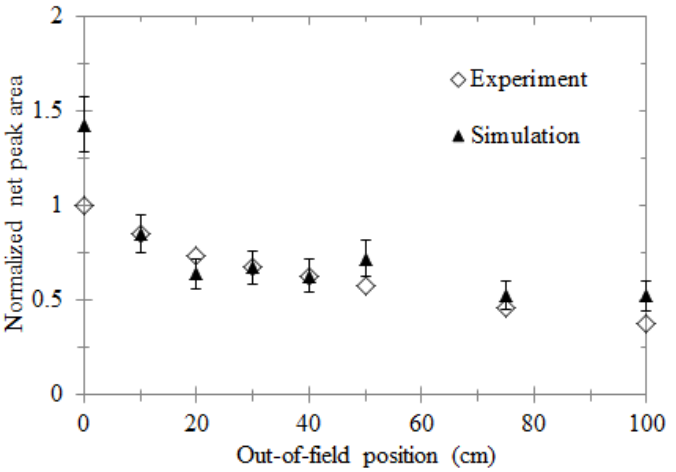

Fig. 12. Comparison between simulated and measured photoneutron profiles for 20 MV photons, simulation model corrected, activation detector containing a foil of vanadium.

C. Energy spectrum and average emission intensity

Energy spectra of photoneutrons emitted by the Saturne 43F medical accelerator were determined by simulation. They are similar to the ones obtained for the SAPHIR facility accelerator. As an example, Fig. 13 shows result obtained for the 12 MV photon model. Mean energy is around 1 MeV. Average emission intensities were calculated by counting the number of neutrons crossing a sphere surrounding the accelerator. Statistical uncertainties on these calculations are lower than 0.01%. After having multiplied these results by the number of electrons delivered per second by the accelerator (6.25×10^{16} for 12 MV photons and 1.88×10^{17} for 20 MV photons), the pulse duration (4 µs) and the frequency (100 Hz), we found average emission intensities of 1.61×10^{9} and 8.75×10^{10} neutrons per second considering 12 MV and 20 MV photons respectively.

Same methodology from the one presented for the SAPHIR accelerator was applied to evaluate energy spectra and average emission intensities. However, due to long simulation times, absolute activation calculations were carried out using one (n,γ) cross-section library only: ENDL-92. Overall uncertainty on pulse duration, frequency and electron current peak intensity was assumed to be negligible since the Saturne 43F is a metrological accelerator. Correction factor of 8% was taken into account to reduce simulated absolute detection efficiency as we used the same germanium detector at SAPHIR and Laboratoire National Henri Becquerel. We used ENDF/B-VII tungsten photonuclear cross-sections. However, as different materials are involved in the emission of photoneutrons for this accelerator, no correction factor on tungsten cross-section threshold errors [6] were included in our calculations. For 20 MV photons, statistical uncertainties associated to (n,γ) reaction rates were lower than 7% for the activation detector in position 0 cm and lower than 12% when the latter was in an out-of-field position. For 12 MV photons, they were respectively lower than 10% in the photon field and lower than 15% out-of-field. Average values on ratios between simulated and experimental net peak areas were determined for out-of-field positions. Our results are gathered in Table V.

Generally speaking, tendencies are the same that the ones obtained previously for the accelerator of the SAPHIR facility. Simulations underestimate experiments and, as expected, large disagreements emerge when considering low electron energies. Our results for 12 MV photons illustrate the impact of both tungsten cross-sections threshold errors and inaccurate photonuclear cross-section evaluations. Factor on the order of ten is reached. Furthermore, measurements could have enabled to determine directly the neutron dose delivered by the accelerator. However, neither a ^{252}Cf [19] or ^{241}Am-Be source [20] was available to calibrate the activation detector to neutron dose. Moreover, smaller activation detector of the size of bubble detectors [21] could enable to increase spatial resolution in the photon field, while offering the possibility of being easily simulated in comparison with such bubble detectors.

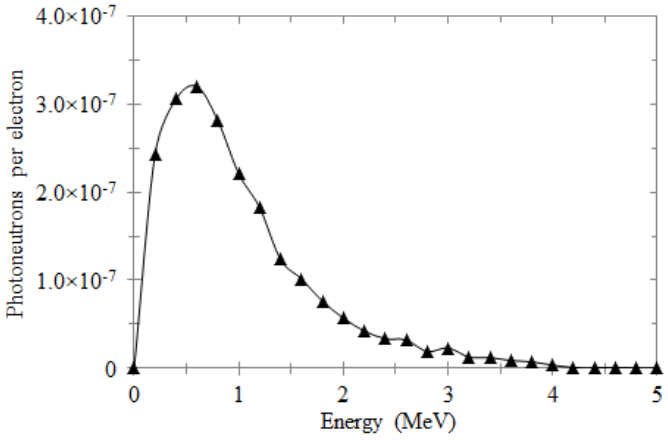

Fig. 13. Energy spectrum of the photoneutron flux emitted by the Saturne 43F accelerator for 12 MV photons.

TABLE V
RATIOS BETWEEN SIMULATED AND EXPERIMENTAL NET PEAK AREAS CARRIED OUT FOR THE ACTIVATION DETECTOR CONTAINING A FOIL OF VANADIUM, SILVER, OR ALUMINUM, CONSIDERING THE SATURNE 43F MEDICAL ACCELERATOR PRODUCING 12 MV OR 20 MV PHOTONS. SIMULATIONS CARRIED OUT USING ENDL-92 (n,γ) CROSS-SECTIONS.

	12 MV photons			20 MV photons		
	V	Ag	Al	V	Ag	Al
Field	0.12	-	-	0.79	-	0.83
Out-of-field	0.11	-	-	0.61	0.95	-

V. CONCLUSIONS AND OUTLOOK

In this paper, we report a photoneutron flux characterization methodology based on an activation detector. The advantages of such detector are the following: inexpensive, fast to deploy, and easy to simulate. On the other hand, we have identified that, when the detector is exposed to high-energy photons, spurious neutrons are produced in the cadmium surrounding the detector and the foil. However, the part of the signal measured due to spurious photoneutrons can be determined through simulation.

Discrepancies encountered between absolute activation simulations and measurements have been investigated. We identified that there is a strong probability for the latter to be due to poor knowledge of photonuclear cross-sections in the energy range of interest. Thus, even if models are validated for photon dose calculations, estimation by simulation of photoneutron production in medical accelerators leads to underestimated results. Regarding photoneutron production by the electron accelerator of the SAPHIR facility, our study achieved good confidence in the knowledge of the photoneutron flux characteristics. New developments of neutron interrogation with an electron accelerator could now be performed with the help of simulation taking into account a new correction factor on tungsten or tantalum photonuclear cross-sections undervaluation.

ACKNOWLEDGMENT

The authors are very grateful to Dr. L. Le Noir De Carlan for allowing access to the Saturne 43F accelerator located at Laboratoire National Henri Becquerel. We would also like to thank Dr. B. Poumarède and Dr. J.-M. Bordy for their support to our measurement campaign on the medical accelerator.

REFERENCES

[1] C. Ongaro *et al.*, "Analysis of photoneutron spectra produced in medical accelerators," *Phys. Med. Biol.*, vol. 45, L55-L61, 2000.
[2] W. L. Huang, Q. F. Li, Y. Z. Lin, "Calculation of photoneutrons produced in the targets of electron linear accelerators for radiography and radiotherapy applications," *Nucl. Instrum. Methods Phys. Res. B*, vol. 229, pp. 339-347, 2005.
[3] J. L. Jones *et al.*, "Photonuclear-based, nuclear material detection system for cargo containers," *Nucl. Instrum. Methods Phys. Res. B*, vol. 241, pp. 770-776, 2005.
[4] L. Lakosi, C. Tam Nguyen, E. Serf, "Neutron interrogation of shielded/unshielded uranium by a 4 MeV linac," *Appl. Radiat. Isot.*, vol. 69, pp. 1251-1254, 2011.
[5] F. Jallu *et al.*, "The simultaneous neutron and photon interrogation method for fissile and non-fissile element separation in radioactive waste drums," *Nucl. Instrum. Methods Phys. Res. B*, vol. 170, pp. 489-500, 2000.
[6] A. Sari *et al.*, "Detection of actinides with an electron accelerator by active photoneutron interrogation measurements," *IEEE Trans. Nucl. Sci.*, vol. 59, no. 3, pp. 605-611, 2012.
[7] L. D. Stephens and A. R. Smith, University of California Radiation Laboratory Rep., UCRL-8418, 1958.
[8] J. F. Briesmeister, MCNP—A General Monte Carlo N-Particle Transport Code—Version 4C, Los Alamos National Laboratory Rep., LA-13709-M, 2000.
[9] J. S. Hendricks, MCNPX Extensions Version 2.5.0, Los Alamos National Laboratory Rep., LA-UR-04-0570, 2004.
[10] G. Audi, O. Bersillon, J. Blachot, A. H. Wapstra, "The NUBASE evaluation of nuclear and decay properties," *Nucl. Phys. A*, vol. 729, pp. 3-128, 2003.
[11] Database ENDF/B-VII.1 [online]. Available: http://www.nndc.bnl.gov/exfor/endf.htm
[12] F. Carrel *et al.*, "Measurement of plutonium in large concrete radioactive waste packages by photon activation analysis," *IEEE Trans. Nucl. Sci.*, vol. 57, no. 6, pp. 3687-3693, 2010.
[13] M. I. C. Cataldi, E. Wolynec, M. N. Martins, P. Gouffon, Y. Miyao, "Electrodisintegration of ^{208}Pb, ^{209}Bi and ^{181}Ta," *J. Phys. G: Nucl. Phys.*, vol. 14, pp. 779-786, 1988.
[14] K. Kosako *et al.*, "Angular distribution of photoneutrons from copper and tungsten targets bombarded by 18, 28, and 38 MeV electrons," *J. Nucl. Sci. Technol.*, vol. 48, pp. 227-236, 2011.
[15] G. Tosi *et al.*, "Neutron measurements around medical electron accelerators by active and passive detection techniques," *Med. Phys.*, vol. 18, pp. 54-60, 1991.
[16] Database CNDC [online]. Available: http://www-nds.iaea.org/photonuclear/other_files/cndc/
[17] Database ENDF/B-VII.0 [online]. Available: http://www.nndc.bnl.gov/exfor/endf.htm
[18] Database ENDF/B.VI.8 [online]. Available: http://www.nndc.bnl.gov/exfor/endf.htm
[19] R. C. McCall, Neutron Radiation from Medical Electron Accelerators, Stanford Linear Accelerator Center Rep., SLAC-PUB-2739, 1981.
[20] E. Carinou, I. E. Stamatelatos, V. Kamenopoulou, P. Georgolopoulou, P. Sandilos, "An MCNP-based model for the evaluation of the photoneutron dose in high energy medical electron accelerators," *Physica Medica*, vol. XXI, pp. 95-99, 2005.

[21] L. Bourgois, D. Delacroix, A. Ostrowsky, "Use of bubble detectors to measure neutron contamination of a medical accelerator photon beam," *Rad. Prot. Dos.*, vol. 74, pp. 239-246, 1997.